PCCP

Accepted Manuscript

ROYAL SOCIETY OF CHEMISTRY

www.rsc.org/pccp

On the macromolecular cellulosic network of paper: changes induced by acid hydrolysis studied by NMR diffusometry and relaxometry

Allegra Conti[‡], *Giovanna Poggi*[§], *Piero Baglioni*[§]*, *Francesco De Luca*[‡]*

[‡] CNR-IPCF UOS and Department of Physics, "Sapienza" University of Rome, p.le A. Moro 2, 00185 Rome, Italy

[§] Department of Chemistry and CSGI, University of Florence, via della Lastruccia 3, 50019, Sesto Fiorentino (Florence), Italy

Abstract

The cellulosic network of artificially acidified paper has been studied by 2D NMR relaxometry, NMR diffusometry and NMR diffusion-diffraction. Results show that the acidifying treatment enlarges the macropore structure of paper increasing the pore connectivity and modifying the exchange between water populations localized in amorphous cellulose. Acidification damage suggests that simple breaking of the amorphous portion of fibrils occurs. Nevertheless, under a specific acidifying condition, a rearrangement in cellulose network seems to take place, with a reduction of the average macropore size and a loss of pore connectivity. The identification of water populations by 2D relaxation maps allows for monitoring the changes in cellulose water mobility due to the depolymerization process. In general the relaxation and self-diffusion results confirm that water mobility increases with acidification.

Keywords: Paper, NMR diffusometry, cellulose, acid hydrolysis, T1-T2 correlation maps

1. Introduction

Paper is a stochastic network of cellulose fibers aggregated in a quasi-planar arrangement.[1] Fibers, which have lateral size on the μm scale, are formed by microfibrils, which in turn are aggregates of elementary fibrils. Microfibrils can reach diameters up to about 40 nm, while elementary fibrils have lateral size ranging from 3 to 15 nm. Elementary fibrils seem to constitute a sort of natural cellulose unity specific of cellulose source species.[2] The formation of microfibrils from elementary fibrils is explained in terms of a coalescent mechanism that reduces the free energy of elementary fibril surfaces.[3] Therefore, microfibril size may change according to the characteristics of their formation environment.[4] From elementary fibrils to fibers, the bonding mechanisms are mainly based on hydrogen bonds and Van der Waals interactions.[1] Fiber aggregation occurs by the so-called Campbell effect.[1]

Elementary fibrils in cotton paper are composed to a large extent (up to 70%) of ordered cellulose crystallites and to a lesser part of amorphous cellulose domains (ACDs). Therefore, a single cellulose chain, which is built from repeated D-glucopyranose units linked by 1,4-β-glycoside bonds, passes through a sequence of crystallites and ACDs. Because of fiber crossover, the three-dimensional view of paper shows a complicate structure made of pores and channels, with a variety of sizes and percolation pathways, which shape the fluid transport properties of a paper sheet.[1]

The main gates of water-cellulose interaction are the ACDs. Here water either forms hydrogen bonds with the OH groups of cellulose chains or it bridges OH groups of different chains, therefore modulating the chain extension and inducing mechanical stress on fibrils. Since external water can reach the amorphous zone by means of pore connectivity, the hydration

mechanism of paper depends not only on the pore size distribution, but also on its topological properties.[5]

Degradation of cotton-based paper is primarily the result of cellulose chain breaking by hydrolysis, that is, the scission of the β-1,4-glycosidic bonds of cellulose chains.[6,7] This reaction is catalyzed by acids and requires the availability of water. The hydrolysis generally starts in the ACDs and slows down, or it ends at all, at amorphous-crystalline interfaces (ACIs) where cellulose chains' density increases due to chain packing, which "prepares" the crystalline region.[8] The tight crystallites formed by cellulose chains are impenetrable to water. Therefore depolymerization of cellulose involves amorphous cellulose only, ending at the so-called leveling-off degree of polymerization, which corresponds to chain length comparable to the size of the crystalline regions in fibrils.[9–11]

Acid hydrolysis in historical paper is triggered by several factors, including atmospheric pollution,[12] sizing compounds employed in papermaking such as alum and rosin,[13] and writing fluids such as the highly corrosive iron and metal gall inks.[14] Acid-catalyzed hydrolysis affects almost every paper sheet produced since the 18th century, threatening the integrity of historical documents, drawings or other cellulose-based works of art.[15]

In this article the changes induced by hydrolysis on cellulose chains arrangement and how this process influences the hydration mechanism of paper are studied. While the fundamental mechanisms of hydrolysis in cellulose fibers have been explained, details concerning cellulose rearrangement due to hydrolysis progress are not fully clear yet.[8] A better understanding of physical processes underlying the degradation of paper by hydrolysis may provide new insights about the water-cellulose interaction. Moreover, the comprehension of these mechanisms may help clarifying the interaction between acidic paper and deacidifying agents, such as alkaline

nanoparticles,[16–19] in order to refine restoration and preservation strategies of degraded cellulose-based works of art. To simulate the changes induced by acid-catalyzed hydrolysis, samples of paper made of pure cellulose have been acidified at different pH and characterized by 2D NMR correlation relaxometry[20], NMR diffusometry[5] and by NMR diffusion-diffraction.[21]

Molecular self-diffusion and correlation measurements of relaxation times T_1 (longitudinal) and T_2 (transverse) allow for obtaining information about the mobility and exchange characteristics of water populations in cellulose.[20,22] The degree of cellulose polymerization characterizes both the confinement conditions for water and the number of water-exposed OH groups.

The diffusivity of water may also give indirect insight about the rearrangement of cellulose as a result of hydrolysis processes, since the confinement condition of molecules change in response to the variation in the degree of polymerization (DP). However, when sizes on the μm scale have to be monitored in an interconnected porous medium, the NMR excitation time parameters are experimentally demanding, as they require both μs time-scale setting to observe the free diffusion of water inside the pore and ms time-scale setting to observe the confinement effect, being the change between free and restricted diffusion regime what allows establishing the pore size.[21] In this case, however, the NMR diffusive-diffraction effect proves particularly useful since confinement size may appear, in opportune conditions, as a diffraction-like modulation of the gradient stimulated-echo (PFG-STE) signal of water.[21]

2. Experimental methods

2.1 Sample Preparation

Whatman filter paper (grade 5; 125 mm diameter) composed of cotton raw fibers (minimum α-cellulose[1] content of 98%) was used for the preparation of artificially acidified samples. *Ac1* samples were obtained by immersing 10 filter papers in 1 liter of H_2SO_4 (pH=1) for 3 hours. *Ac1n* samples were subsequently obtained by immersing *Ac1* samples in MilliQ water (resistivity: 18MΩ at 25°C) for 6 hours after acidification, in order to remove residual sulfuric acid. *Ac2* samples were obtained by immersing 10 filter paper in 1 liter of H_2SO_4 (pH=3) for 3 hours. *Ac2n* samples were finally recovered by immersing *Ac2* samples in MilliQ water for 6 hours after the acidification, in order to remove sulfuric acid again. Sulfuric acid (96%) was supplied by Carlo Erba. The untreated filter paper, used as a reference system, is indicated as the *TQ* sample. Since capillarity and pore size could be altered by dunking paper into water,[5] the comparison between *Ac1*, *Ac1n*, *Ac2*, *Ac2n* and *TQ* was made homogeneous by treating *TQ* like the *Ac1* and *Ac2* samples, but with distilled water only: this allows for comparison between samples, so preventing effects from mere soaking.

After the acidification, the viscosimetric DP was determined with the cuprylethylenediamine method[23] by a Ubbelohde viscometer. Cuprylethylenediamine was supplied by Sigma-Aldrich. DP values are reported in Table 1. The experimental error associated to these measurements is ± 50 units.

Ion chromatography was carried out to quantify residual sulfates in samples using a Dionex DX-120 chromatograph equipped with a Dionex Ion Pac AG4A (4×50 mm) guard column and a Dionex Ion Pac AS4A (4×250 mm) separation column (eluent: Na2CO3/NaHCO3 1.8 mM at 1.1 mL min^{-1}). A Dionex ASRS-Ultra II 4-mm self-regenerating suppressor was used before the conductivity cell. Variable amounts of paper (from 10 mg to 500 mg) were extracted in 15 g of MilliQ water. In order to favor the extraction, samples were sonicated in an ultrasonic bath (Falc)

at 59 kHz for one hour, and then left under stirring for 24 hours. Before being injected in the chromatographic columns, water extractions were filtered through a 0.45 μm filter. Sulfates amounts in samples are reported in Table 1. The experimental error associated to these measurements is about 10%.

NMR measurements were performed 28 days after samples preparation. Before measurements, samples were kept at 22±1 °C for 24 hours in a controlled relative humidity (RH) environment to get both 100% RH and a 45% RH hydrated sample set. Samples were sealed in a plastic film to avoid water loss during NMR measurements.

2.2 NMR measurements

2D NMR correlation relaxometry measurements were performed using a single-sided Bruker Profiler working at about 0.4 T.[24] The resonance condition is established in a sensitive volume of about 2.0x0.2x0.8 cm^3 onto the probe surface. The pulse sequence used for T_1-T_2 correlation experiments was *[saturation-*τ_1*-90°-*t_E*/2-(180°-*t_E*/2-acquisition-*t_E*/2)*$_n$*-*τ_{rd}*]*$_m$ with a recycle delay time τ_{rd} =2 s, an echo time t_E=44 μs and a number of echoes n=500.[25] The saturation time (τ_1) varies *m* times in geometric progression from 0.1 ms to 4 s, with an increment factor 1.3 and with 1024 scans per each value.

This sequence allows obtaining a (*nm*) matrix giving the magnetization:

$$M\left(\tau_1, t_E\right) = M_0 \iint P\left(T_1, T_2\right) k_1\left(\tau_1, T_1\right) k_2\left(k_2, T_2\right) dT_1 dT_2 \qquad (1)$$

where M_0 is the equilibrium magnetization, $k_{1,2}$ the relaxation kernels and $P(T_1,T_2)$ the T_1-T_2 correlation distribution, which is obtained by inverse Laplace transform of $M\left(\tau_1, t_E\right)$.[26]

Diffusion measurements were performed by a Brucker Avance 300 MHz spectrometer equipped with a BGU2 gradient unit that generates a maximum gradient intensity of about 1200 G/cm. The sequence used is the PFG-STE[27], where G gradients of δ duration (δ≅1.4 ms) are applied between three 90° pulses. The first two pulses are separated by a time interval τ≅2.0 ms and the second pulse has a delay Δ from the third; Δ works as a spin flying time. For each of the 20 gradient steps, during which the gradient intensity was increased from zero to 1050 G/cm, 32 scans were performed. The relaxation recycle delay has been fixed to 3 s. The sample of hydrated paper has been cut in strips of about 2.5x20 mm^2; after being sealed in a plastic film, six of these strips were inserted in the NMR tube for measurements. The relaxation times at 300 MHz are indicatively more than 10 times the relaxation times at low field.

The dynamic wave vector $\vec{q} = \gamma\delta\vec{G}$ and Δ evolution of PFG-STE signal for free water are given by

$$E(q,\Delta) = E(0,\Delta)\exp\left\{-q^2 D(\Delta - \delta/3)\right\} \quad (2)$$

where D is the molecular self-diffusion coefficient. In case of restricted diffusion regime, $E(q,\Delta)$ changes, according to the confinement size, in relation with Δ, G and D.[21]

2.3 Weight measurements

Weight measurements were performed with a Sartorius BP211D balance with 0.01 mg resolution. The balance was equipped with a glass case with 100% RH at 22±1 °C. Before measurements, samples were hydrated for 24 hours at 22±1 °C in a 45% RH environment.

3. Results and Discussion

The attenuation of the PFG-STE ratio $E(q,\Delta)/E(0,\Delta)$ versus q^2 (Eq. 2) shows a linear behavior in semi-log scale when unrestricted diffusion regime runs.[21] The experimental results show that, already at Δ=10 ms, water is in restricted diffusion regime in all samples. An example can be seen in Fig. 1, where the PFG-STE data of *Ac1* are reported. As it will be shown below, the *Ac1* sample possesses the largest confining regions for water.

As stated above, under the restricted diffusion regime information about confining dimensions can be obtained by NMR diffusion-diffraction measurements. However, because of both pore connection and pore heterogeneity, the diffraction condition is more complex than the simple limit $\Delta >> \frac{a^2}{D}$, where a describes the pore size, strictly valid for an enclosing pore.[21] In particular, the heterogeneity of shapes and sizes of pores makes the intensity of diffraction modulation poorly resolved, due to the superposition of signals from the whole distribution of confining geometries.[21,28,29] Nevertheless, it is possible to discern diffraction dips from noise effects by a statistical criterion, which allows for assessing when difference between $E(q,\Delta)/E(0,\Delta)$ ratios of adjacent qs are statistically significant in comparison to the error distribution.[28]

The diffraction patterns $E(q,\Delta)/E(0,\Delta)$ vs q at Δ=40 ms are reported in Fig. 2, for all 100% RH hydrated samples. The same results of Fig. 2 have been also obtained for different Δs in the range 30-60 ms.

The smallest q related to diffraction dips gives information about the largest water confining structures. The higher qs, on the other hand, have to be ignored since they undergo the effect of modulation tangling related to the diffraction patterns of the smaller confining structures. This effect and the limit imposed by T_2 relaxation allow for only assessing confining size on the μm scale. Therefore, diffraction measurements concern mainly the effect of amorphous cellulose domain breakage on macroporosity. Even though the amorphous domains are in the mesoporous range (amorphous domain length: 25-50 nm; crystallites length: 50-150 nm),[2] due to their large number it is expected that they alter the macroporosity in a detectable way.

The largest confining lengths d turn out to be: $d(TQ)\cong 2.1$ μm (grade 5 paper is supplied by Whatman as a 2.5 μm particle retention size filter; measurements on non soaked *TQ* give the same d), $d(Ac2n)\cong 2.3$ μm, $d(Ac2)\cong 1.5$ μm, $d(Ac1n)\cong 3.1$ μm, $d(Ac1)\cong 4.8$ μm. The resolution of 0.1 μm fulfills the statistical criterion mentioned above.[28] These results show that acid-catalyzed hydrolysis tends to enlarge the confining space of water; this is especially the case of the *Ac1* sample, which has a DP corresponding to about the leveling-off DP.[2]

The *Ac2* sample behaves in a different way. d of *Ac2*, in fact, seems appreciably smaller than the one of *TQ*. This result probably indicates that a rearrangement of cellulose fragments takes place through the formation of hydrogen bonds between their OH groups, perhaps also involving intact chains and water, so producing a sort of shrinkage of macropores by a mechanism opposite to the one indicated for macropore enlargement. Conditions for pore shrinkage might depend by several parameters as, for example, fragments mobility, excluded volume of fragments or geometrical frustration effects,[30] which probably are all favorable to the formation of hydrogen bounds between fragments only in the specific conditions of the *Ac2* sample. However, a detailed

analysis of pore shrinkage occurrence requires a suitable experimental approach and it has to be postponed to a specific work.

The dependence of the PFG-STE signal on the self-diffusion coefficient is well fitted in any 100% RH sample with the equation

$$E(q,\Delta) = E_{0S}(\Delta)\exp[-q^2 D_{eS}(\Delta - \frac{\delta}{3})] + E_{0F}(\Delta)\exp[-q^2 D_{eF}(\Delta - \frac{\delta}{3})] \qquad (3)$$

where two diffusion components appear, each with a suitable effective self-diffusion coefficient D_{eS} and D_{eF}; the subscripted *S* and *F* stand for slow and fast component, respectively. The effective self-diffusion coefficient is the NMR-measured one in restricted diffusion regime and depends on Δ.[21] The behavior of $D_{eF}(\Delta)$ and $D_{eS}(\Delta)$ in the *Ac1* sample is reported in Fig. 3.

The fast diffusive water component is always the major fraction in all samples. E_{0F} is about 60% in *TQ*, 65% in *Ac2n*, 77% in *Ac2*, 75% in *Ac1n* and 75% in *Ac1*. Moreover, the qualitative relations $D_{eF}(Ac1) > D_{eF}(TQ) \cong D_{eF}(Ac1n) \cong D_{eF}(Ac2n) > D_{eF}(Ac2)$ and $D_{eS}(Ac1) \cong D_{eS}(TQ) \cong D_{eS}(Ac1n) \cong D_{eS}(Ac2n) \cong D_{eS}(Ac2)$ keep valid for each Δ (see Tab. 2 for numerical values at Δ=10 ms). These results suggest that there are two water populations having different mobility: a larger one associated to more mobile water, and a smaller one associated to more restricted water. These evidences are confirmed by relaxation data reported below. When the restrict diffusion regime holds, the effective self-diffusion coefficients are, however, strictly related to pore sizes. Water in large pores shows higher effective self-diffusion coefficient than in small pores, therefore in this case the apparent mobility of water is a mirror of pore size.[21]

Moreover, while for interconnected pores the effective self-diffusion coefficient reaches a finite asymptotic value for $\Delta \to \infty$, in isolated pores it tends to zero.[21] Fig. 3 clearly shows this trends for the *Ac1* sample (this trend is common to all samples): the fast component resides in large pores with good connectivity and levels off at high D_{eF} for $\Delta \to \infty$, while the slow component reaches a very low effective self-diffusion coefficient when $\Delta \to \infty$. According to these results, the fast water population may be associated to large and interconnected pores, while the slow one to smaller and poorly connected pores. Within the fast mobile population, however, a hierarchy may also be established based on pore sizes: the stronger confining condition is shown by the *Ac2* sample while the weaker one by the *Ac1* sample.

Also from the self-diffusion point of view the *Ac2* sample behaves in an anomalous way. It shows, in fact, the smallest D_{eS} and D_{eF} within samples. These results confirm the findings of diffraction data in Fig. 2.

The interconnection of pores may be quantified by assessing the so-called tortuosity, which is the reciprocal of pore connectivity. The tortuosity, α, is defined by the relation[21]

$$\lim_{\Delta \to \infty} \frac{D_e(\Delta)}{D_0} = \frac{1}{\alpha} \qquad (4)$$

where D_0 is the self-diffusion coefficient measured in unrestricted regime, that is $D_{0S}=D_{eS}(\Delta \to 0)$ and $D_{0F}=D_{eF}(\Delta \to 0)$. The $\Delta \to 0$ coefficient values are experimentally inaccessible. However, what is of interest here, it is the change of tortuosity of treated samples with respect to *TQ*. This comparison can be done by assuming that D_{0S} and D_{0F} do not depend on sample characteristics. Since free diffusion means diffusion measured for Δ short enough that

water molecules do not experiment confinement constraints (that is in practice the bulk self-diffusion coefficient) the assumption that D_{0S} and D_{0F} have each the same values for all samples can be considered reasonably correct.

Assuming the same unrestricted diffusion coefficients, from eq. (4) it is possible to valuate ratios like $R_{S,F}(Ac1)=\frac{D_{eS,F}(\infty)_{Ac1}}{D_{sS,F}(\infty)_{TQ}}=\frac{\alpha_{S,F}(TQ)}{\alpha_{S,F}(Ac1)}$ which give the connectivity of a sample, in this case *Ac1*, with respect to *TQ*. The results are reported in Tab. 3.

Data of Tab. 3 show in finer detail how the connectivity changes with hydrolysis progress. Where the DP varies greatly, as in *Ac1*, the connectivity significantly increases; where DP variation is small, as in *Ac1n* and *Ac2n* samples, a small modification of connectivity is observed. Once more, *Ac2* shows an anomalous behavior: R_S<1 indicates that its connectivity is reduced with respect to *TQ*. In Fig. 4, the relationship between connectivity and *d* is shown. Even though diffraction data do not allow for separating water into fast and slow components - in this view all water is in restricted diffusion regime, while confinement sizes can not be fully disentangled from dips - Fig. 4 confirms that the stronger the hydrolysis action, or the larger *d*, the higher the connectivity. The increase in connectivity mirrors an increase in interpore channel size, probably due to the disordered arrangement of cellulose fragments produced by hydrolysis. When fragments tend to aggregate to form local structure, as it has been conjectured for *Ac2*, a reduction of connectivity is expected.

The *Ac1* sample, which has the largest confining structures, shows the highest connectivity, while as *d* decreases the connectivity gets smaller. This also suggests that acid hydrolysis simply "opens" amorphous cellulose cavities in microfibrils without a reorganization of cellulose fragments. It is interesting to note that also the connectivity of structures related to slow water component increases, even though in a minor way.[8] Since the acid action is reduced when the

crystallites are approached,[9–11,31] the fast water component has to be associated to water in the ACDs,[22] while the slow component to water in the ACIs.[20] The diffusivity as well as the connectivity, seen by the ACI-water component, are less dependent on sample treatment.

As stated above, the *Ac2* sample shows, also for connectivity, the same anomalies observed in diffraction patterns. While the fast component of *Ac2* returns a reduced connectivity when compared to *Ac2n*, and similar to *TQ*, the slow one shows an evident reduction with respect to both *Ac2n* and *TQ*: it seems, as conjectured above, that cellulose in *Ac2* get reorganized, involving the ACI sites as well.

The characteristic hygroscopicity of paper is mainly ascribed to the possibility that external water reaches the amorphous sites of fibrils.[32] In this view, *Ac2* should therefore present a reduction of hygroscopicity with respect to *TQ* and the *Ac1* samples, because of its reduced overall connectivity and a possible reduction of exposed OH groups due to cellulose rearrangement, while it is expected that *Ac1* exhibit the highest hygroscopicity. These different behaviors have been confirmed by weight measurements, reported in Fig. 5, where it is interesting to note that an appreciable difference between *TQ* and *Ac2* is mainly observed at long time, as expected by the reduced R_S of *Ac2*.

Also the T_1-T_2 NMR correlation maps (Fig. 6) show two different water populations: a higher T_2 one, which is therefore characterized by more mobile water, and a lower T_2 population, which is characterized by less mobile water. Diffraction and diffusion results, as well as data reported by Lepore et al.,[20] allow the assignation of the upper T_2 spots to ADCs water and the lower T_2 spots to ACIs water. This assignation is further confirmed by the comparison between the maps of 100% and 45% (Fig. 7) RH hydrated samples. All spot maxima have almost the same T_1; this

indicates that the rotational dynamics of water doesn't change appreciably within populations because, as expected, microscopic interactions of water are similar in ADCs and ACIs.

As in multi-phases system, some exchange occurs between water populations. When fast or quasi-fast exchange regime run, the exchange relaxation averaging leads the T_2 of each phase to shift towards an average value which depends on the spin population of each phase.[33]

In the 100% RH samples the T_2 of peaks of the bottom spots are centered on almost the same value (about 0.1 ms) that characterizes the homologous spots in the 45% RH hydrated samples, while upper spots of the former are centered on T_2 values higher than those retrieved in the latter. T_2 of upper spot (T_{2u}) and bottom spot (T_{2b}) peaks for both sample series are reported in Fig. 8. It is clear that the increase in T_{2u} in the 100% RH samples is due to the greater availability of external and mobile water. This is confirmed by the larger ratios between upper and lower spot peak intensities in the 100% RH samples with respect to 45% RH ones, where ratios are close to unity: external water mainly accesses the ACDs, while water in the ACIs remains fairly unaltered. The fast and slow water fractions, as obtained from relaxation maps, are in very good agreement with the fast and slow water fractions obtained by self-diffusion measurements (Fig. 9).

Therefore the 100% RH samples return maps where both the increase in the upper spots intensity and the shift of T_{2u} only towards higher values with respect to 45% maps (Fig. 8) indicate that exchange occurs mainly between ACD water and water from outside. On the other side, the 45% RH relaxation maps give indication that exchange occurs mainly between ADCs and ACIs water, both because the amplitude of the upper and bottom spots are similar and because the T_{2u}s are lower than those of the 100% hydrated samples (Fig. 8). The *Ac1* sample (Fig. 7-E), in particular, shows the more effective exchange between ADCs and ACIs water

populations, as the maxima of the two spots shift significantly towards one another with respect to peak positions of all the others 45% RH hydrated samples. This, apart from confirming that protons involved in the NMR maps are from water, shows that acid hydrolysis may facilitate the exchange between water populations, because of the increase of porous structure connectivity (Fig.4).

Fig. 8 shows that every 100% RH treated sample has a higher T_{2u} than *TQ*. Apart from confinement and exchange, other effects must be invoked to fully explain the relative values of T_{2u} within samples, being $T_{2u}(Ac2n) > T_{2u}(Ac2) \approx T_{2u}(Ac1n) > T_{2u}(Ac1) \approx T_{2u}(TQ)$.

The presence of residual water from the sample neutralization process may partially justify the conditions $T_{2u}(Ac1n) > T_{2u}(Ac1)$ and $T_{2u}(Ac2n) > T_{2u}(Ac2)$. On the other hand, this conjecture is not able to explain why $T_{2u}(Ac1) \approx T_{2u}(TQ)$ and $T_{2u}(Ac2) \approx T_{2u}(Ac1n)$. In order to fully explain the T_{2u} behavior, the presence of residual sulfates in samples and, consequently, the different availability of OH groups, must be taken into account.

Ac1 has the largest number of OH groups exposed to water and the highest concentration of sulfate groups remained after the acidification treatment (see Tab. 1). Therefore, even though water in *Ac1* is less confined, its mobility may be reduced by the high probability of binding interactions for SO_4^{2-} ions solvation. This may reduce T_{2u} to a value similar to that of *TQ*.

Even though DP(*Ac2n*)≈DP(*Ac1n*)≈DP(*Ac2*) (Tab. 1), the number of OH groups exposed in the *Ac1n* sample should be larger than those exposed in *Ac2* that shows a reduced porosity. However, the cellulose reorganization in the *Ac2* sample could also reduce the T_2 exchange averaging between upper and bottom spots, therefore resulting in a large T_{2u} value, which is partially compensated by the high SO_4^{2-} concentration. This could explain why $T_{2u}(Ac1n) \approx T_{2u}(Ac2)$. Finally, *Ac2n* present the largest T_{2u} value, probably because all parameters

in this sample (low SO_4^{2-} concentration, small number of exposed OH, residual neutralization water) are favorable to a high T_{2u}.

3. Conclusions

The cellulosic network of artificially acidified samples was studied by NMR 2D correlation relaxometry and NMR diffusometry. From diffusion-diffraction dips, changes in the macropore structure of paper, due to the acidifying treatments, have been monitored while information about water mobility[34] have been extracted from T_1-T_2 correlation maps.

In particular, it has been shown that a strong acidifying treatment enlarges the macropore structure of paper leading to an increase of pore connectivity, therefore favoring the exchange between water populations residing in the ACDs and in the ACIs. The increase of connectivity, however, makes the "communication" between the microscopic structure of paper and the external world more efficient, therefore increasing the risk of pollutant penetration inside the paper, which may trigger new degradation mechanisms or enhance the acidification process itself. While strong acidification damage seems to suggest that a simple breaking of the amorphous portion of fibrils occurs, with a consequent enlargement of the macropore structure of paper, surprisingly, under a mild acidifying condition, a rearrangement in the cellulose network seems to occur, with a subsequent reduction of the average macropore size and a loss of connectivity. Even though the outline of such an occurrence is still in need of a specific study, the present work highlights that it may exist a condition under which cellulose fragments rearrange in metastable condition, which will eventually lead to the complete depolymerization of cellulose, being the acid-catalyzed hydrolysis of cellulose an autocatalytic process.

Nevertheless, the evolution of the depolymerization process from this metastable condition to the leveling-off DP, established by appropriate studies, could help improving the picture about the degradation of paper as well as refining its conservation strategies.

The 2D relaxation maps confirm their effectiveness in monitoring the conservation status of paper. This aspect, together with the use of the low field non-invasive NMR device, may be of particular importance when historical documents, drawings or other cellulose-based works of art are concerned. The identification of water populations helps following the depolymerization process by observation of the water population exchange associated to water spot positioning in the T_1-T_2 plane; it also allows for some monitoring of the hydration dynamics via relative spot intensities. The relaxation results are in full accordance with the diffusion outcomes and they confirm that water mobility increases with acidification, even though, for a complete explanation of water's T_{2u} behavior, the presence of residual sulfates ions from the acidifying treatment must be taken into account. In particular, the presence of large amount of sulfates strongly hinders water mobility, leading to an unexpected decrease in T_{2u} for the *Ac1* sample. Moreover, since T_{2b} does not change appreciably as a consequence of the different treatments applied to paper, relaxation data suggest that the ACI regions are less easily reached by sulfate ions. Only in the case of very strong acidification (*Ac1* sample) remarkable effects are detected on T_{2b}. This seems to suggest that water in these regions is trapped in a more effective way, or, in other words, is less prone to exchange with the external world. This is probably due to the increase in cellulose chain density as the crystalline regions are approached, making them hardly accessible to water, pollutant or chemical agents.

AUTHOR INFORMATION

Corresponding Authors

* Tel. +39-0554573036, baglioni@csgi.unifi.it. Tel. +39-0649913472, francesco.deluca@roma1.infn.it.

ACKNOWLEDGMENT

This work was partly supported by CSGI, and the European Union, Project NANOFORART (FP7-ENV-NMP-2011/282816). The authors would like to thank Dr. Mirko Severi (Department of Chemistry, University of Florence) for the help with the chromatographic measurements. Thanks are due to M. Hurlimann (Schlumberger-Doll Research) who supplied us with the 2D Laplace Inversion Software.

References

1. K. Niskanen, *Paper Physics*, Fapet Oy, Helsinki, 1998.
2. M. Ioelovich, *BioResources,* 2008, **3**, 1403–1418.
3. H. T. Sahin and M. B. Arslan, *Int. J. Mol. Sci.,* 2008, **9**, 78–88.
4. S. Dumitriu, *Polysaccharides: Structural Diversity and Functional Versatility,* Marcel Dekker, New York, 2004.
5. D. Topgaard and O. Söderman, *Langmuir,* 2001, **17**, 2694–2702.
6. D. Fengel, G. Wegener, *Wood: Chemistry, Ultrastructure, Reactions*, Walter De Gruyter, Berlin and New York, 1984.
7. A. Sharples, *J. Polym. Sci.,* 1954, **14**, 95–104.

8. C. H. Stephens, P. M. Whitmore, H. R. Morris and M. E Bier, *Biomacromolecules,* 2008, **9**, 1093–1099.

9. A. M. Emsley, R. J. Heywood, M. Ali and C. M. Eley, *Cellulose,* 1997, **4**, 1–5.

10. P. Calvini, *Cellulose,* 2005, **12**, 445–447.

11. P. Calvini, A. Gorassini and A. L. Merlani, *Cellulose,* 2008, **15**, 193–203.

12. M. C. Area and H. Cheradame, *BioResources,* 2011, **6**, 5307–5337.

13. D. Hunter, *Papermaking through eighteen centuries*, W. E. Rudge, New York, 1930.

14. J. G. Neevel, C. T. J. Mensch and T. J. Cornelis, *ICOM Committee for conservation triennial meeting*, James and James, London, 1999, Vol. 2, 528–533.

15. V. D. Daniels, *Chem. Soc. Rev.,* 1996, **25**, 179–186.

16. R. Giorgi, L. Dei, M. Ceccato, C. Schettino and P. Baglioni, *Langmuir,* 2002, **18**, 8198–8203.

17. R. Giorgi, C. Bozzi, L. Dei, C. Gabbiani, B. W. Ninham and P. Baglioni, *Langmuir,* 2005, **21**, 8495–8501.

18. G. Poggi, R. Giorgi, N. Toccafondi, V. Katzur and P. Baglioni, *Langmuir,* 2010, **26**, 19084–19090.

19. G. Poggi, N. Toccafondi, L. N. Melita, J. C. Knowles, L. Bozec, R. Giorgi and P. Baglioni, *App. Phys. A*, 2013, DOI:10.1007/s00339-013-8172-7.

20. A. Lepore, S. Baccaro, C. Casieri, A. Cemmi and F. De Luca, *Chem. Phys. Lett.,* 2012, **531**, 206–209.

21. P. T. Callaghan, *Translational Dynamics and Magnetic Resonance: Principles of Pulsed Gradient Spin Echo NMR*, Oxford University Press, New York, 2011.

22. I. Viola, S. Bubici, C. Casieri and F. De Luca, *J. Cult. Herit.,* 2004, **5**, 257–261.

23. *UNI 8282: Cellulose in dilute solutions - determination of limiting viscosity number – method in cupri-ethylene-diamine (CED) solution (1994) - equivalent to the ISO standard 5351/1*.

24. B. Blümich, J. Perlo and F. Casanova, *Prog. Nucl. Magn. Reson. Spectrosc.,* 2008, **52**, 197–269.

25. C. Terenzi, C. Casieri and F. De Luca, *Appl. Clay Sci.,* 2011, **53**, 517–524.

26. Y. Q. Song, L. Venkataramanan, M. D. Hürlimann, M. Flaum, P. Frulla and C. J. Straley, *Magn. Reson.,* 2002, **154**, 261–268.

27. S. Peresada, A. Tonielli, R. Morici and C. S. Johnson, *Prog. Nucl. Magn. Reson. Spectrosc.,* 1999, **34**, 203–256.

28. A. M. Torres, R. J. Michniewicz, B. E. Chapman, G. A. R. Young and P. W. Kuchel, *Magnetic Resonance Imaging,* 1998, **16**, 423–434.

29. E. Özarslan and P. J. Basser, *J. Magn. Reson.,* 2007, **188**, 285–294.

30. D. M. Anderson, S. M. Gruner and S. Leibler, *Proc. Nat. Acad. Sci.,* 1988, **85**, 5364-5368.

31. X. Zou, T. Uesaka and N. Gurnagul, *Cellulose,* 1996, **3**, 243–267.

32. T. Kondo and C. Sawatari, *Polymer,* 1996, **37**, 393–399.

33. J. R. Zimmerman and W. E. Brittin, *J. Phys. Chem.,* 1957, **61**, 1328-1333.

34. D. Capitani, M. C. Emanuele, J. Bella, A. L. Segre, D. Attanasio, B. Focher and G. Capretti, *TAPPI,* 1999, **82**, 117-124.

Table 1. DP values and amount of residual sulfates on paper samples.

Sample name	DP	Sulfates ($\mu g/g_{paper}$)
TQ	1080	8
Ac1	127	$50 \cdot 10^3$
Ac1n	857	12
Ac2	826	300
Ac2n	908	6

Table 2. Numerical values of effective self-diffusion coefficient D_{eS} and D_{eF} at Δ=10 ms.

Sample	D_{eS} (10^{-10} m^2/s)	D_{eF} (10^{-10} m^2/s)
TQ	0.2	1.0
Ac1	0.5	2.9
Ac1n	0.2	0.8
Ac2	0.1	0.5
Ac2n	0.3	1.1

Table 3. R_S and R_F of paper samples.

Sample	R_S	R_F
Ac1	3.7	5.9
Ac1n	1.4	1.8
Ac2	0.5	1.0
Ac2n	1.3	1.4

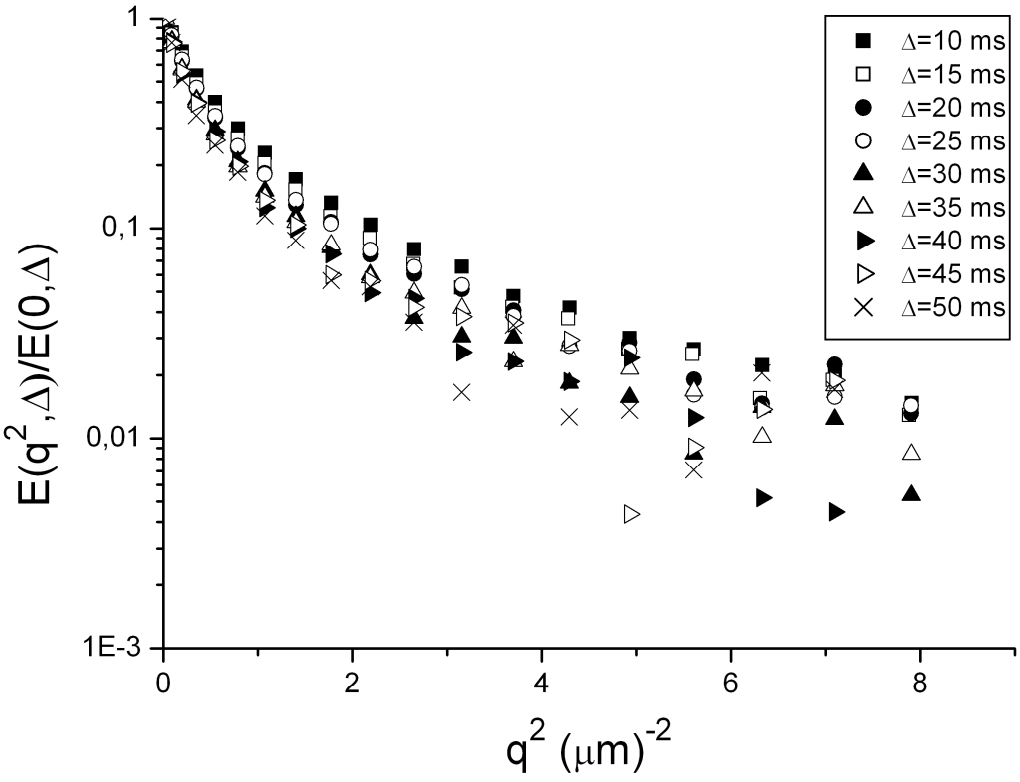

Figure 1. Semi-log scale plot of *E(q, Δ)/E(0, Δ*) vs. *q* at different diffusion times (*Δ*) for the *Ac1* sample. The nonlinear shape of plots marks a restricted diffusion regime for water.

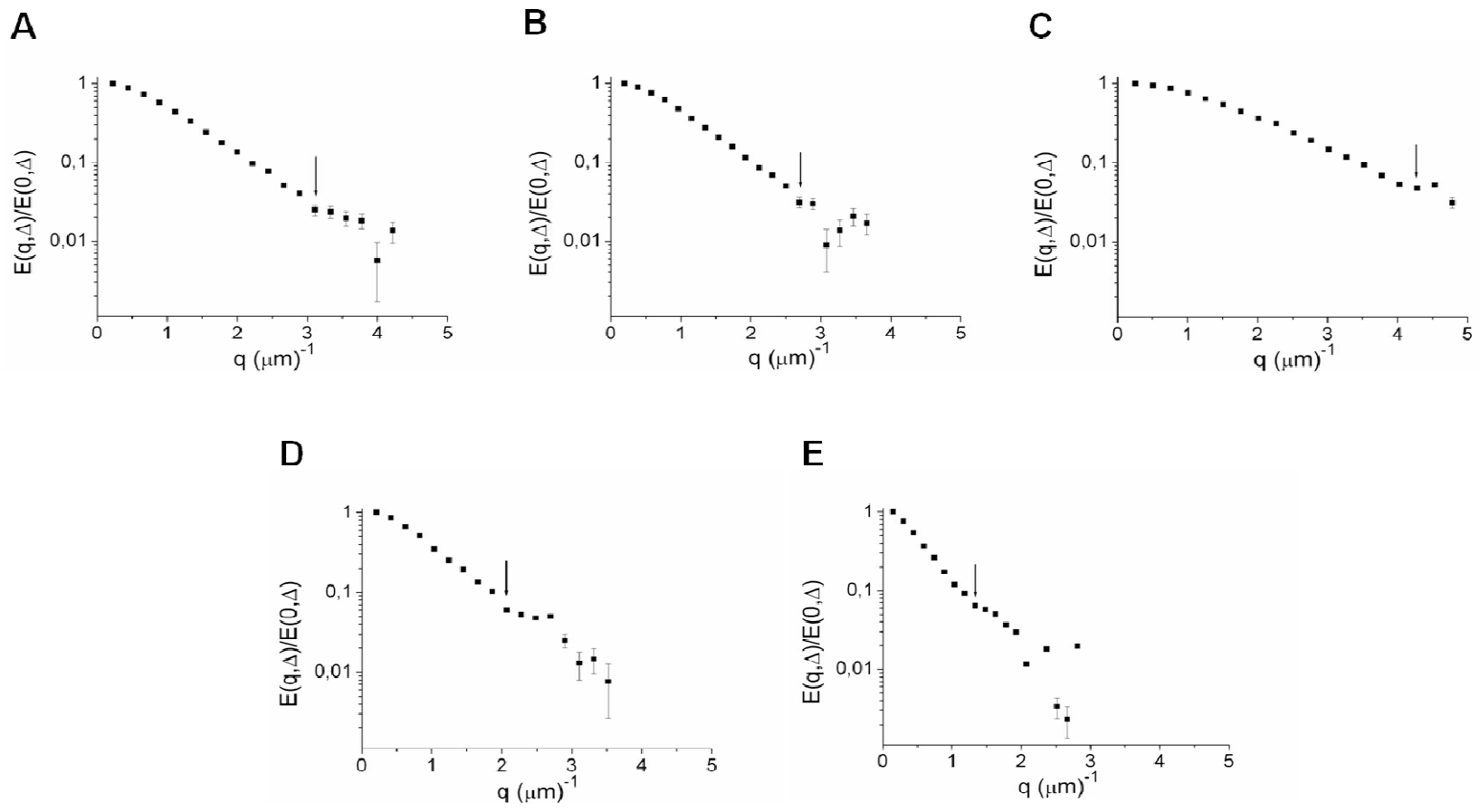

Figure 2. Semi-log plots of $E(q,\Delta)/E(0,\Delta)$ vs q at Δ=40 ms for *TQ* (A), *Ac2n* (B), *Ac2* (C), *Ac1n* (D) and *Ac1* (E). Arrows indicate the first diffraction's dip. The error bars are only indicated where they are larger than the symbol size.

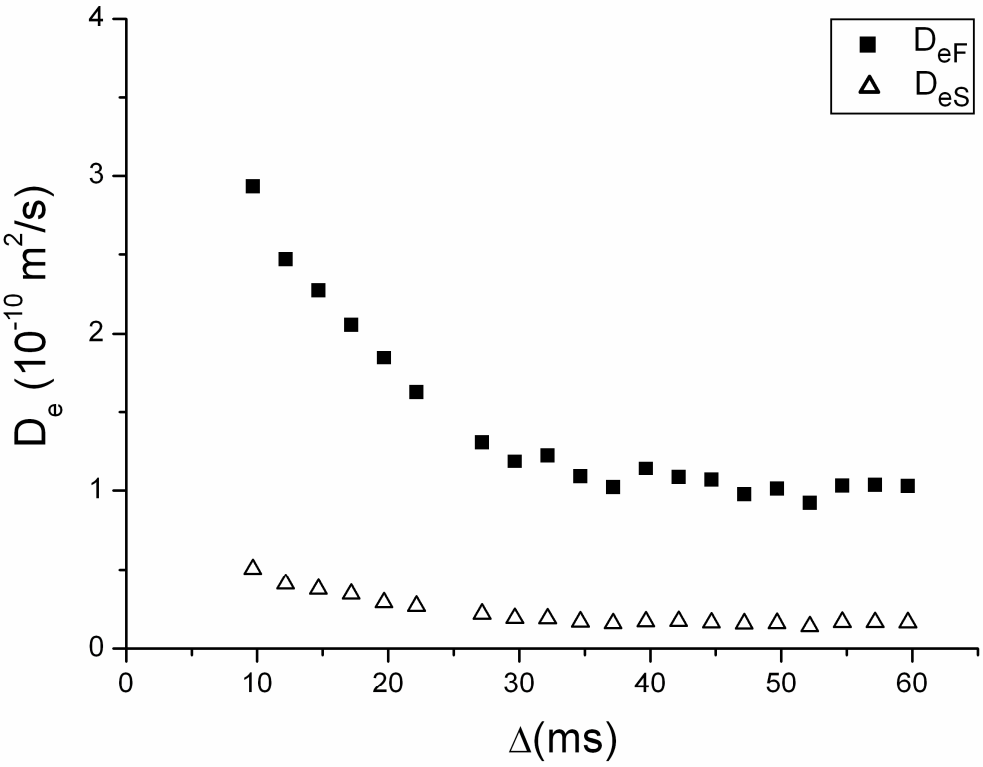

Figure 3. D_{eS} and D_{eF} of water in the *Ac1* sample.

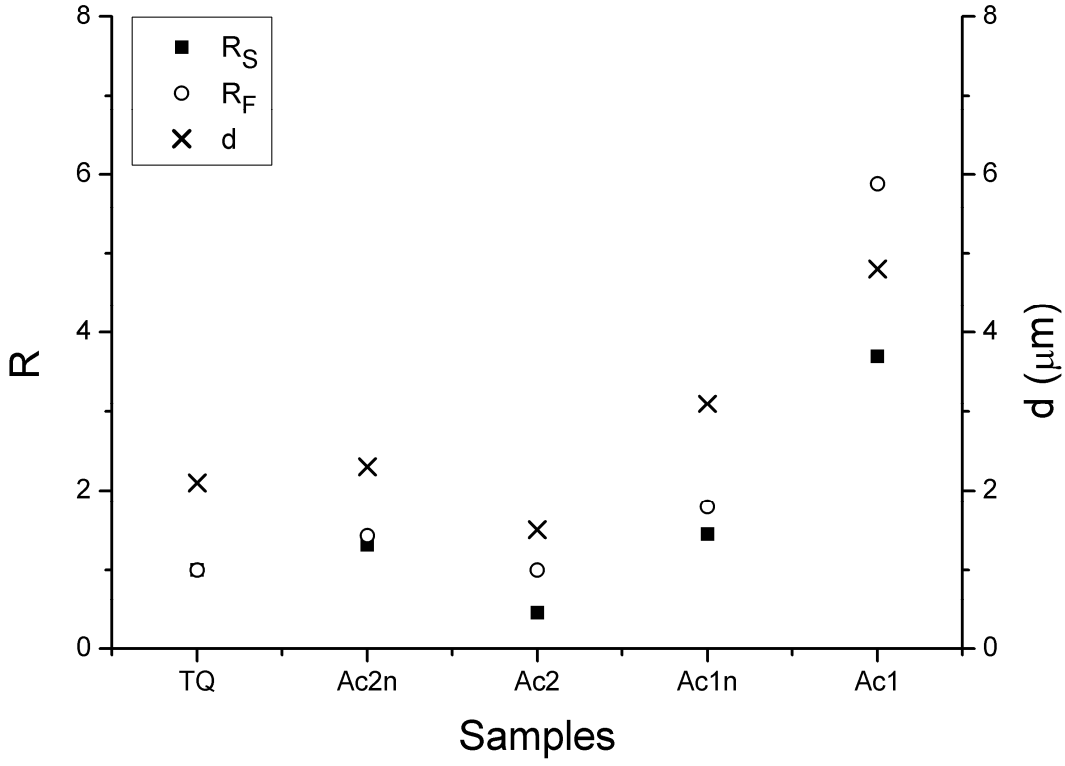

Figure 4. Connectivity ratio (R) and size of the largest confining structure (*d*) of all samples. The correlation between R_S, R_F and *d* is manifest.

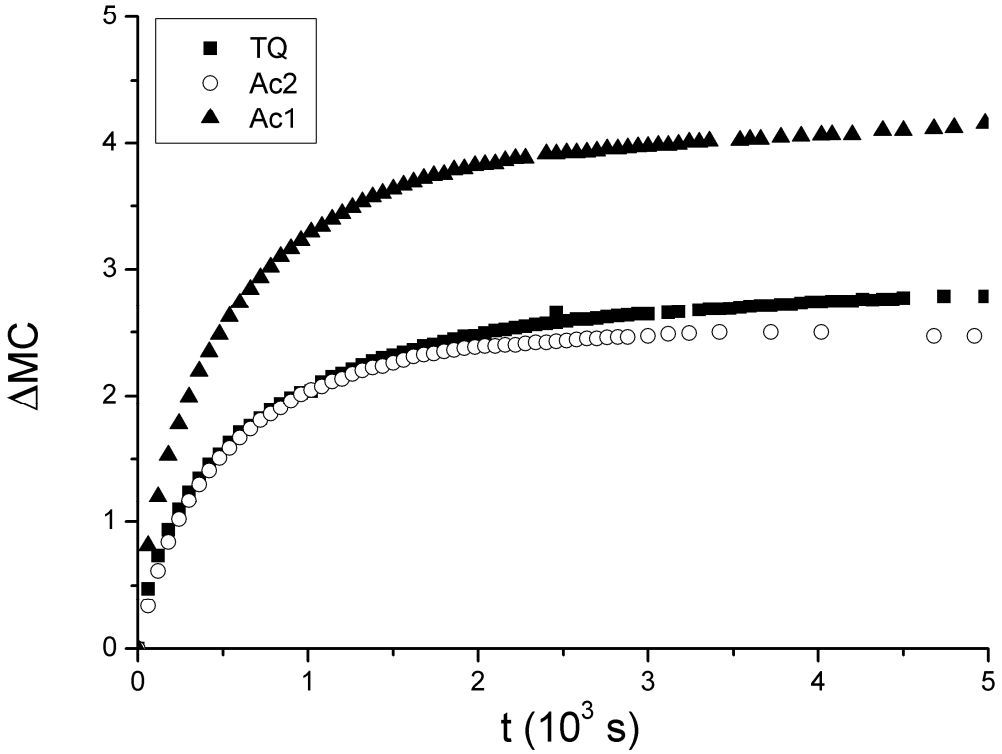

Figure 5. Relative variation ΔMC=[MC(t)-MC(t=0)]/MC(t=0) of moisture content (MC) of samples *TQ*, *Ac1* and *Ac2* as a function of time.

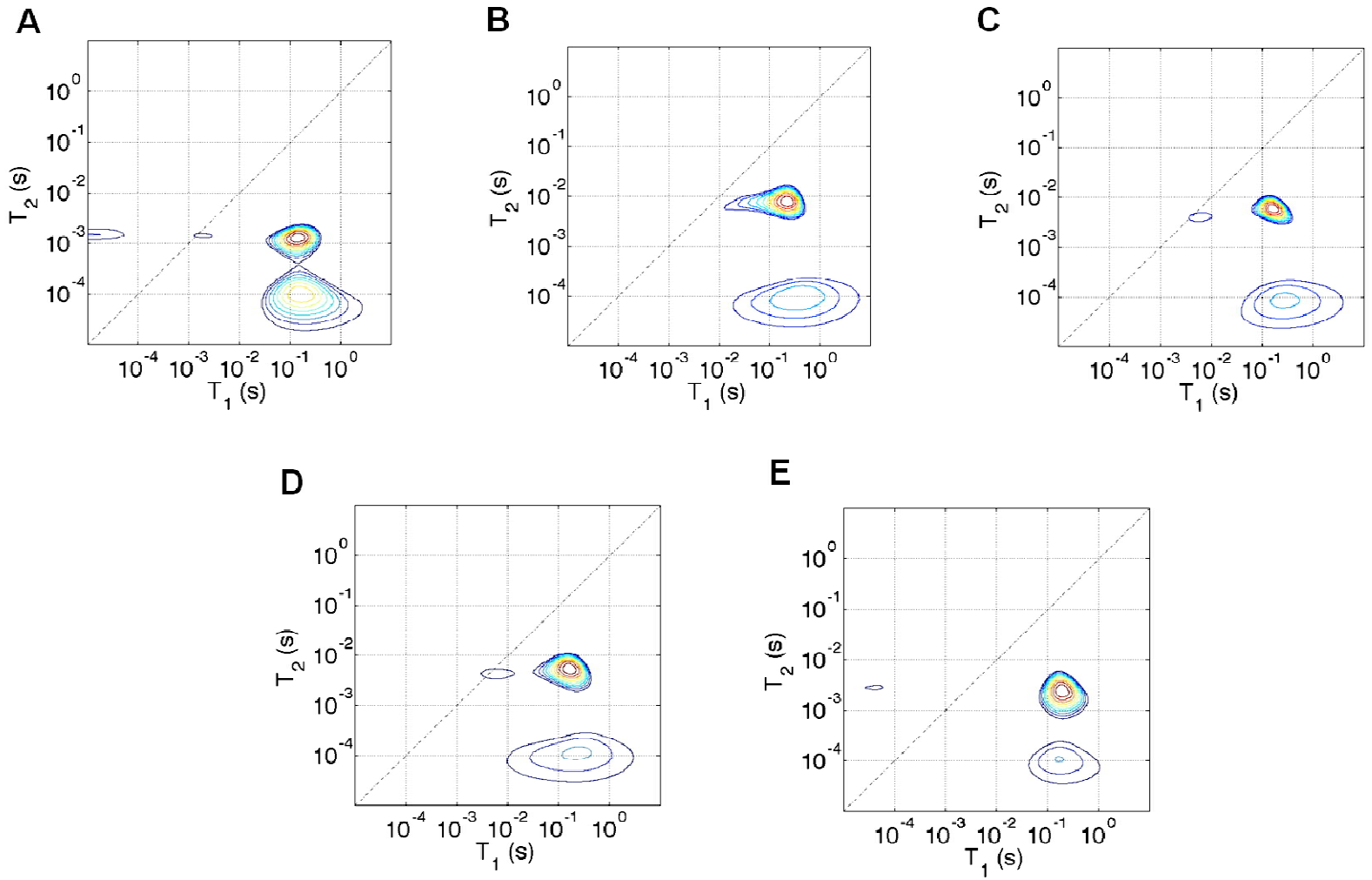

Figure 6. T_1-T_2 correlation maps samples hydrated at 100% RH. A) *TQ*; B) *Ac2n*; C) *Ac2*; D) *Ac1n*; E) *Ac1*.

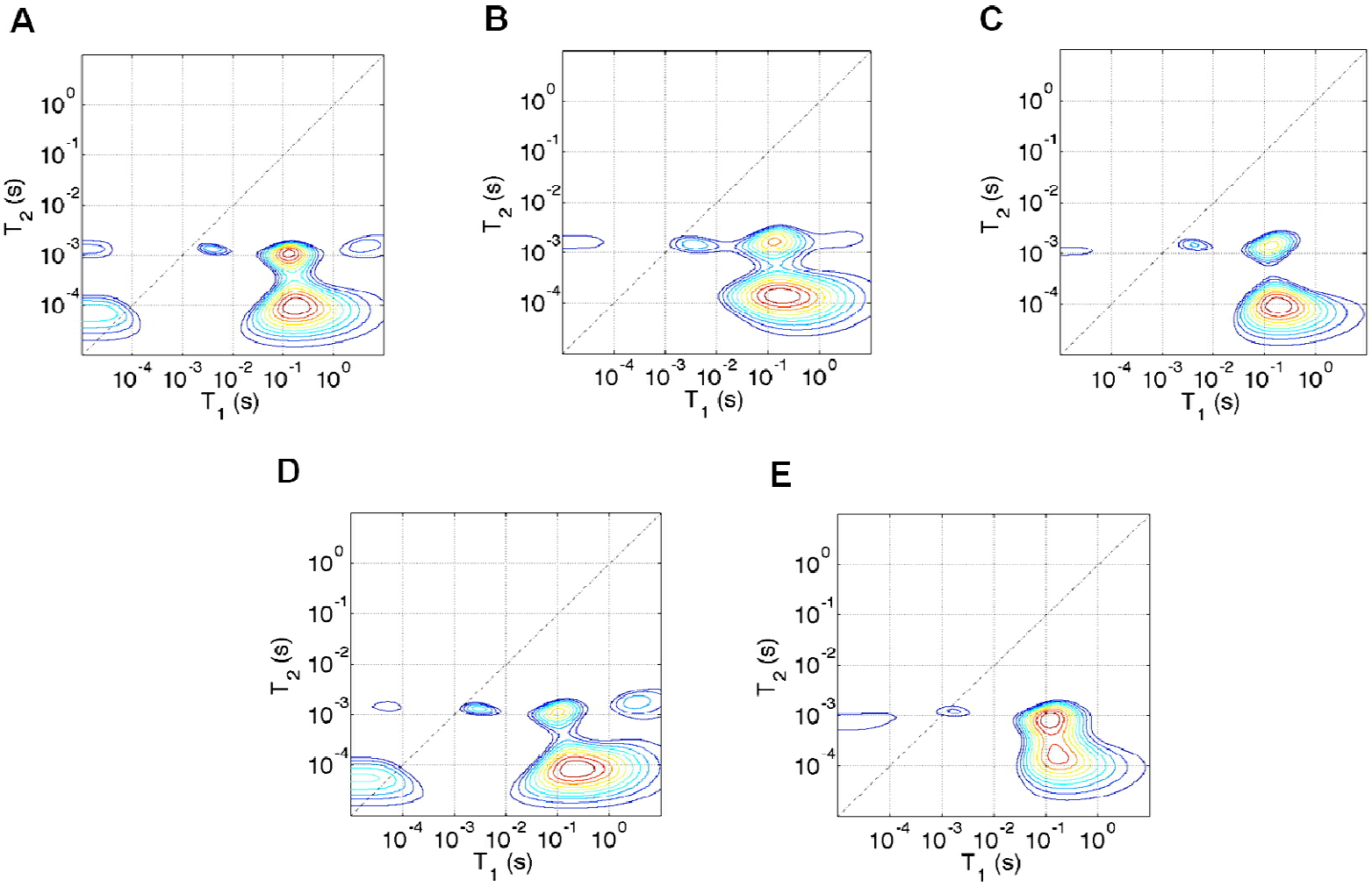

Figure 7. T_1-T_2 correlation maps of samples hydrated at 45% RH. A) *TQ*; B) *Ac2n*; C) *Ac2*; D) *Ac1n*; E) *Ac1*.

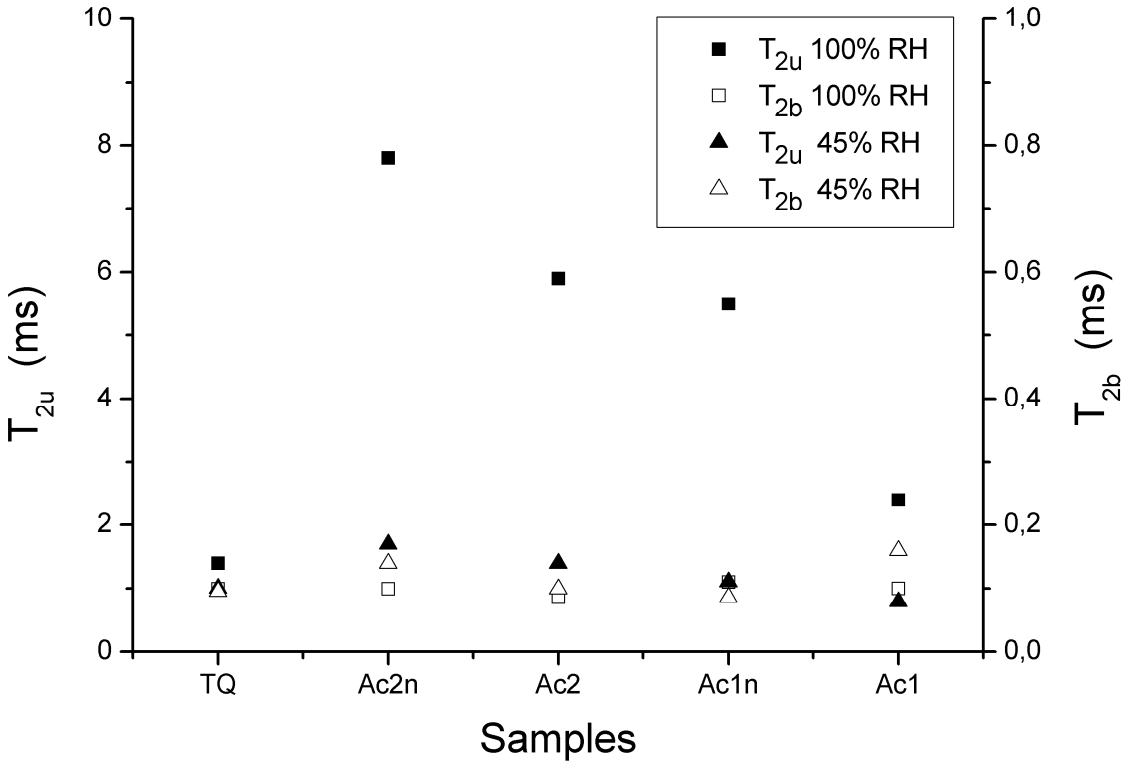

Figure 8. T_{2u} and T_{2d} of 100% RH and 45% RH samples.

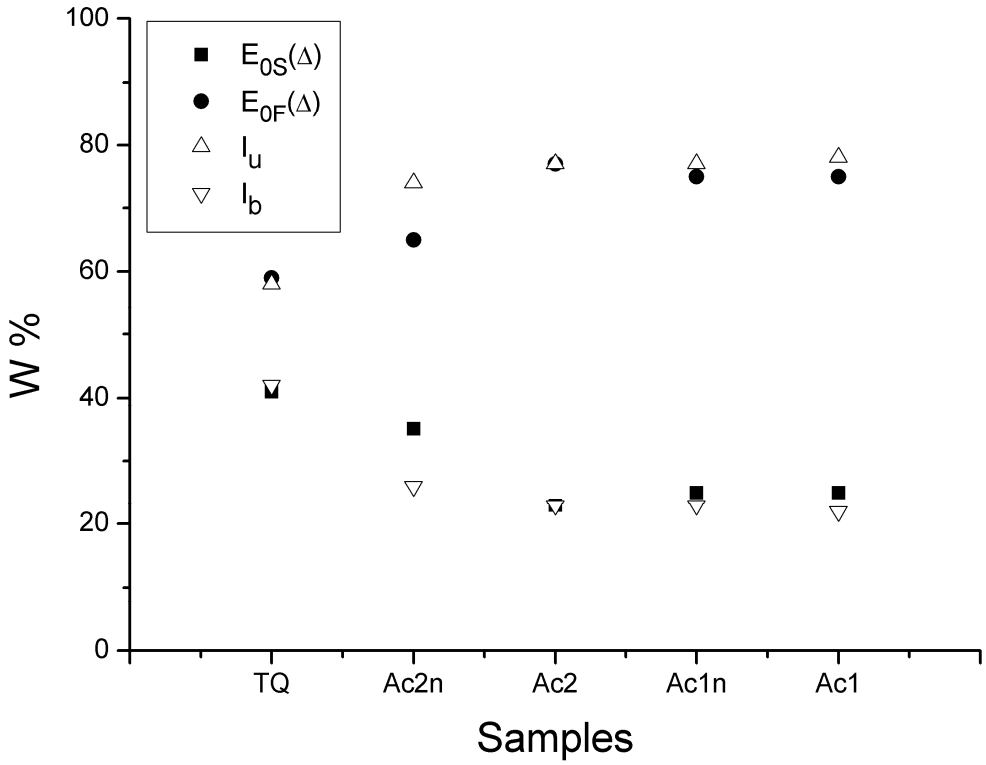

Figure 9. Comparison between the water percentage fractions W% obtained by diffusion measurements ($E_{0S}(\Delta)$ and $E_{0F}(\Delta)$) and by 2D relaxometry (I_u and I_b) in 100% RH samples.

Table of Content entry

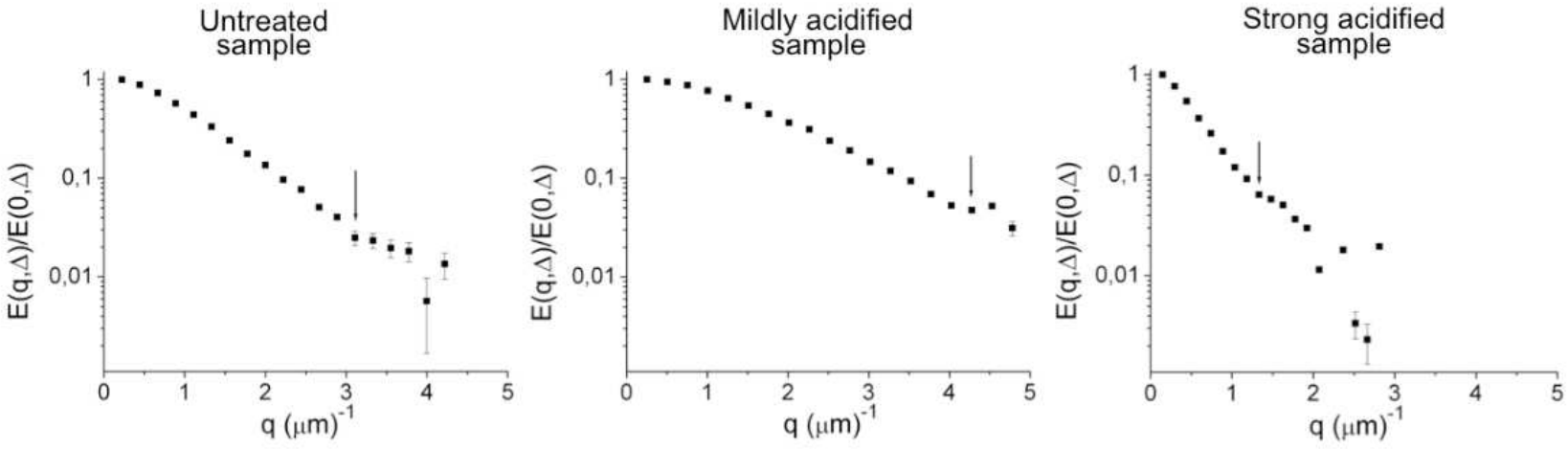

NMR diffusion-diffraction patterns show that in the mildly acidified sample a rearrangement in cellulose network may take place, with a reduction of the average macropore size and a loss of pore connectivity.

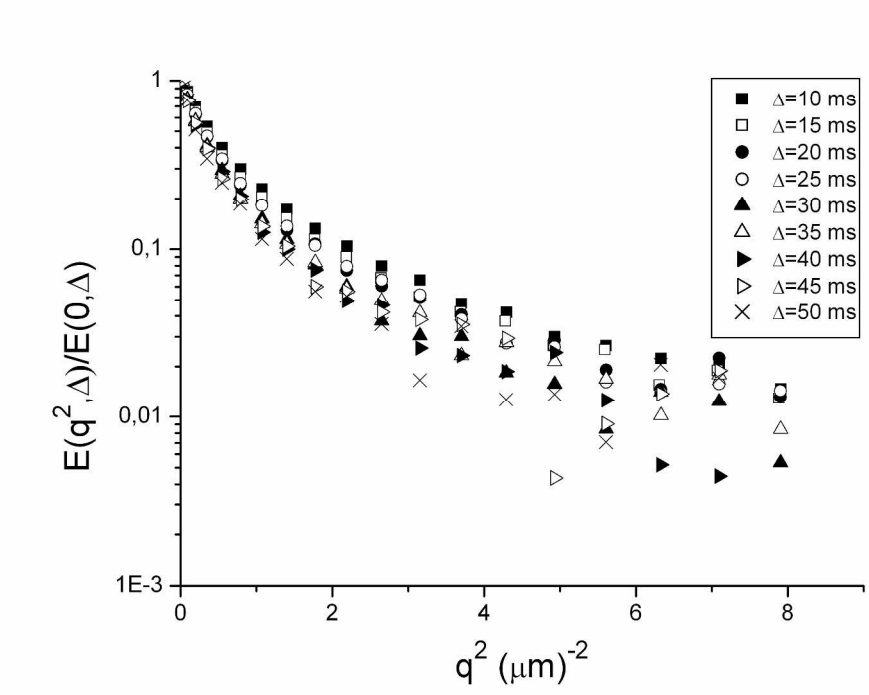

567x399mm (150 x 150 DPI)

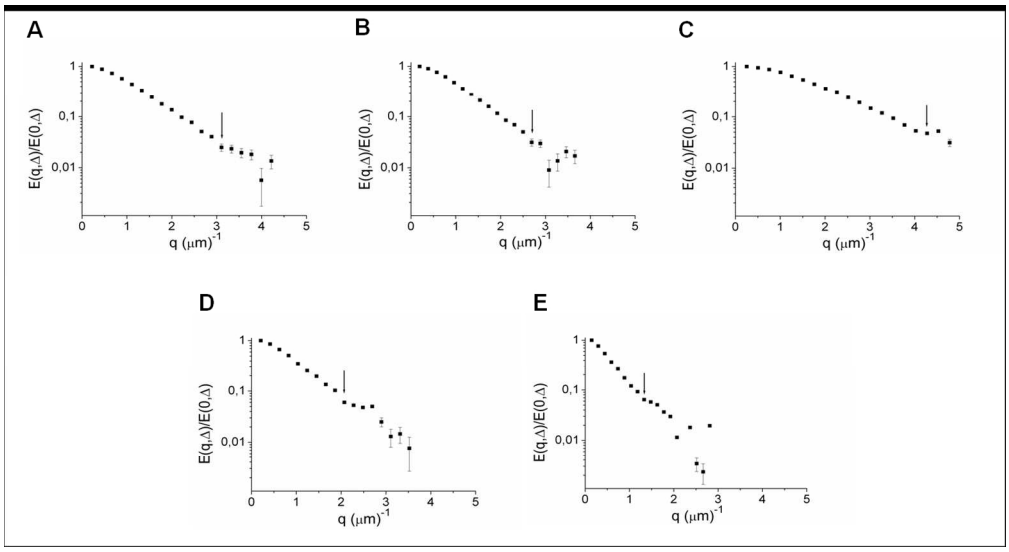

275x149mm (150 x 150 DPI)

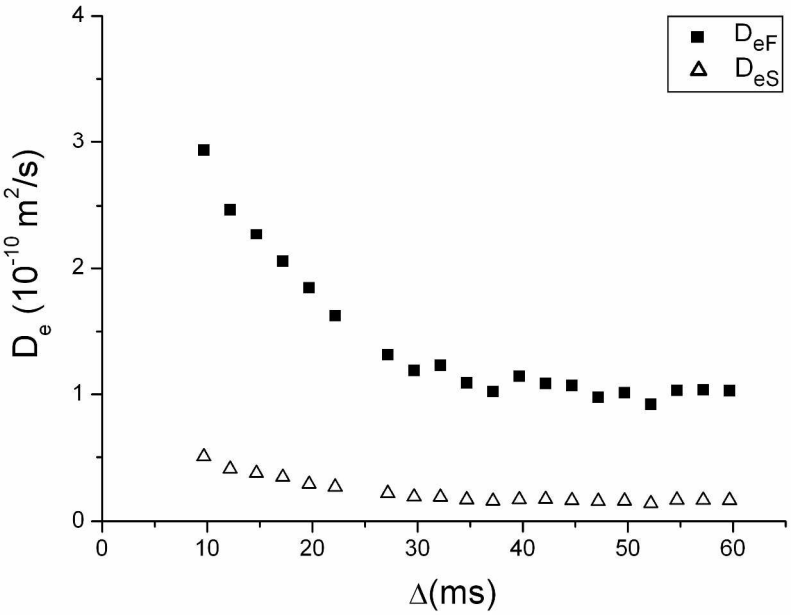

567x399mm (150 x 150 DPI)

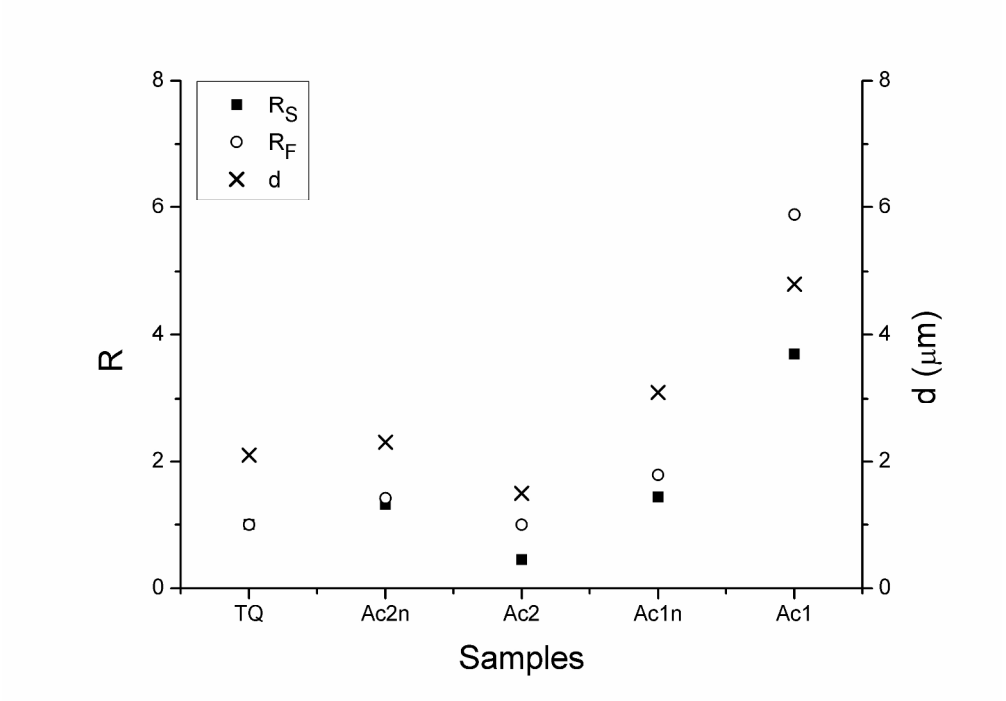

297x210mm (300 x 300 DPI)

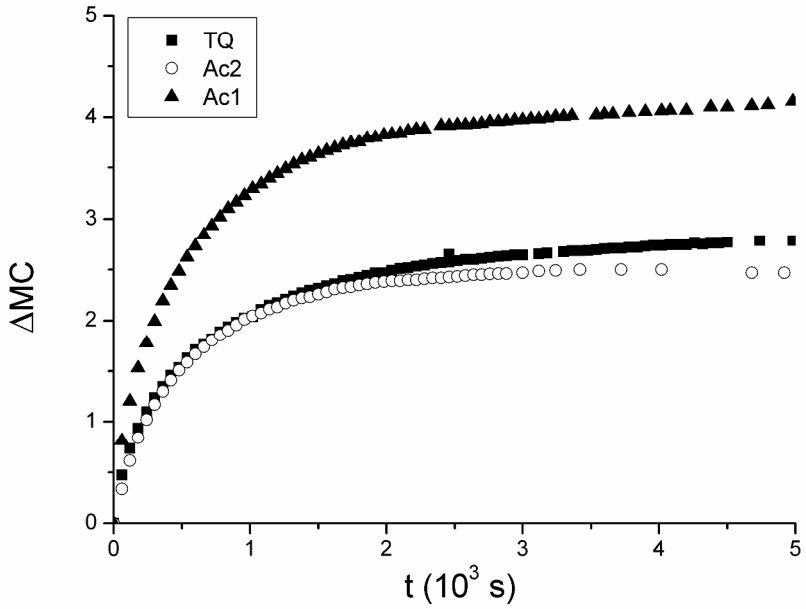

297x210mm (300 x 300 DPI)

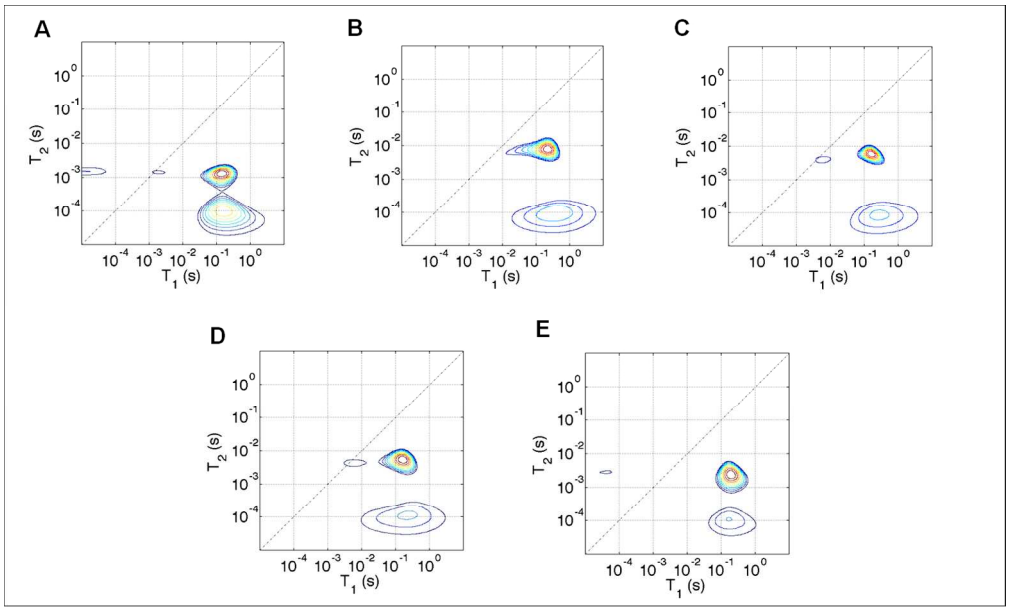

275x165mm (150 x 150 DPI)

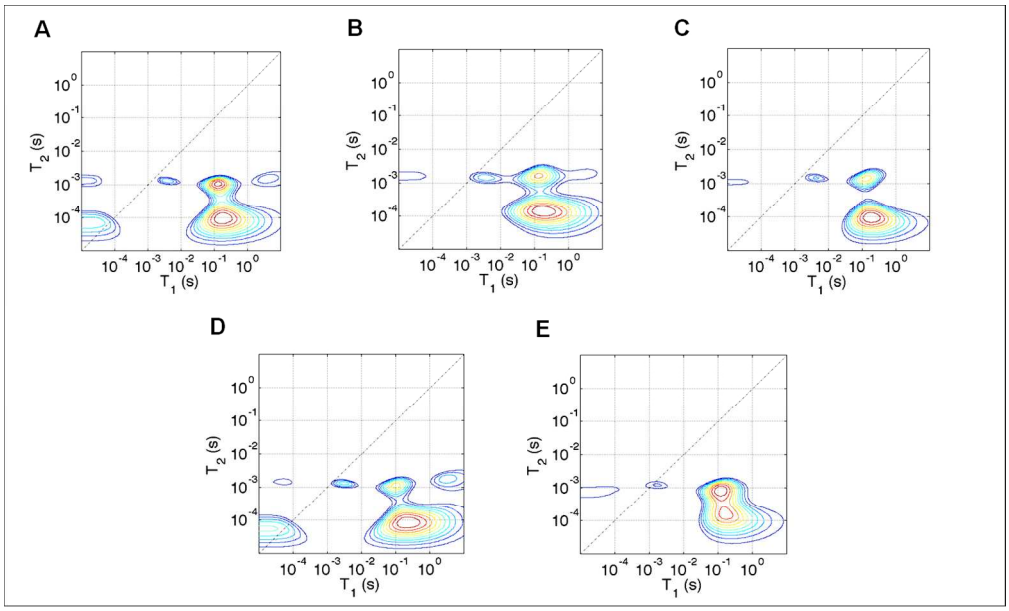

275x165mm (150 x 150 DPI)

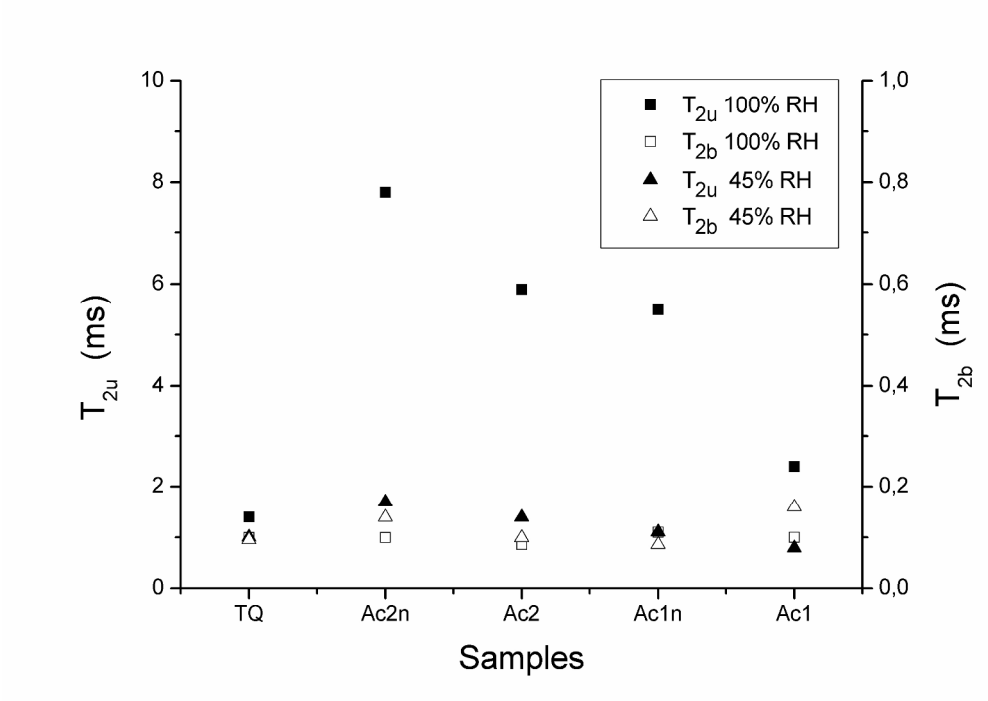

297x210mm (300 x 300 DPI)

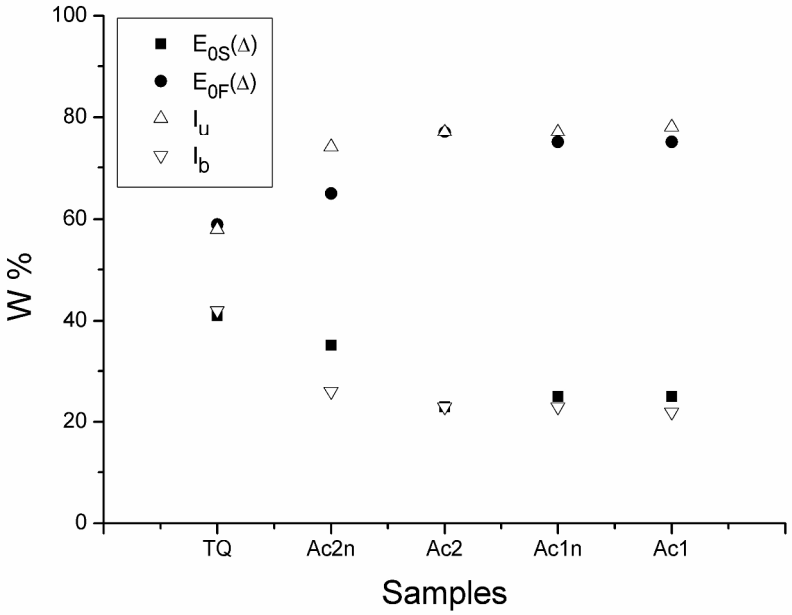

297x210mm (300 x 300 DPI)